

June 2013 Update: Status Report on Assessment of Environmentally Assisted Fatigue for LWR Extended Service Conditions

Summary of

- 1. Room-Temperature Fatigue Test of 316 SS Specimens and Subsequent Data Analysis for Cyclic Plasticity Constitutive Model Development*
- 2. Other Ongoing Experimental and Mechanistic Modeling Activities*

Nuclear Engineering Division

About Argonne National Laboratory

Argonne is a U.S. Department of Energy laboratory managed by UChicago Argonne, LLC under contract DE-AC02-06CH11357. The Laboratory's main facility is outside Chicago, at 9700 South Cass Avenue, Argonne, Illinois 60439. For information about Argonne and its pioneering science and technology programs, see www.anl.gov.

Availability of This Report

This report is available, at no cost, at <http://www.osti.gov/bridge>. It is also available on paper to the U.S. Department of Energy and its contractors, for a processing fee, from:

U.S. Department of Energy
Office of Scientific and Technical Information
P.O. Box 62
Oak Ridge, TN 37831-0062
phone (865) 576-8401
fax (865) 576-5728
reports@adonis.osti.gov

Disclaimer

This report was prepared as an account of work sponsored by an agency of the United States Government. Neither the United States Government nor any agency thereof, nor UChicago Argonne, LLC, nor any of their employees or officers, makes any warranty, express or implied, or assumes any legal liability or responsibility for the accuracy, completeness, or usefulness of any information, apparatus, product, or process disclosed, or represents that its use would not infringe privately owned rights. Reference herein to any specific commercial product, process, or service by trade name, trademark, manufacturer, or otherwise, does not necessarily constitute or imply its endorsement, recommendation, or favoring by the United States Government or any agency thereof. The views and opinions of document authors expressed herein do not necessarily state or reflect those of the United States Government or any agency thereof, Argonne National Laboratory, or UChicago Argonne, LLC.

June 2013 Update: Status Report on Assessment of Environmentally Assisted Fatigue for LWR Extended Service Conditions

Summary of

- 1. Room-Temperature Fatigue Test of 316 SS Specimens and Subsequent Data Analysis for Cyclic Plasticity Constitutive Model Development*
- 2. Other Ongoing Experimental and Mechanistic Modeling Activities*

prepared by
Subhasish Mohanty, William K. Soppet, Saurin Majumdar, and Ken Natesan
Nuclear Engineering Division
Argonne National Laboratory

June 2013

This page intentionally left blank

ABSTRACT

This report provides an update on an earlier assessment of environmentally assisted fatigue for light water reactor (LWR) materials under extended service conditions. This quarterly report is a deliverable in April-June 2013 quarter under the work package for environmentally assisted fatigue in the Light Water Reactor Sustainability (LWRS) program. The overall objective of this LWRS project is to assess the degradation by environmentally assisted cracking/fatigue of LWR materials such as various alloy base metals and their welds used in reactor coolant system piping. This effort is to support the Department of Energy LWRS program for developing tools to predict the aging/failure mechanism and to correspondingly predict the remaining life of LWR components for anticipated 60-80 year operation. The Argonne National Laboratory work package can broadly be divided into the following tasks:

1. Development of mechanistic-based predictive model for life estimation of LWR reactor coolant system piping material (base and weld metals) subjected to stress corrosion cracking and/or corrosion fatigue
2. Performance of environmentally assisted cracking/fatigue experiments to validate and/or complement the activities on mechanistic model development.

There are a number of subtasks under the above-mentioned major tasks. In the reporting period of April-June 2013, the following works were completed:

- Completion of room-temperature fatigue testing of four 316 SS base metal specimens. The resulting data sets were analyzed for cyclic plasticity constitutive model development.
- Room-temperature tensile testing of one 316 SS-316 SS similar metal weld specimen obtained from the fusion zone.
- Room-temperature fatigue testing of one 316 SS-316 SS similar metal weld specimen obtained from the fusion zone.
- Augmenting fatigue test set-up for elevated temperature testing.

The report is organized into two major sections such as:

- Room-temperature fatigue test of 316 SS specimens and subsequent data analysis for cyclic plasticity constitutive model development
- Ongoing experimental and mechanistic modeling activities

This page intentionally left blank

TABLE OF CONTENTS

June 2013 Update: Status Report on Assessment of Environmentally Assisted Fatigue for LWR Extended Service Conditions	ii
ABSTRACT	i
Table of Contents	iii
List of Figures	iv
Abbreviations	vi
Acknowledgments	vii
1 Introduction	1
2 Room-Temperature Fatigue Test of 316 SS Specimens and Subsequent Data Analysis for Cyclic Plasticity Constitutive Model Development	2
2.1 Introduction	2
2.2 Fatigue testing of 316 SS base metal specimens and resulting data analysis	2
2.2.1 Hysteresis behavior of 316SS base metal	3
2.2.2 Evolution of cyclic elastic modulus	7
2.2.3 Evolution of cyclic maximum (σ_n^{\max}) and minimum (σ_n^{\min}) peak stress	9
2.2.4 Evolution of cyclic elastic strain range ($\Delta\varepsilon_n^e$) and plastic strain range ($\Delta\varepsilon_n^p$) ..	10
2.2.5 Evolution of cyclic back stress (α_t)	13
2.2.6 Evolution of damage state (d_t)	16
2.3 Constitutive model for cyclic plasticity	17
2.3.1 Detailed evolutionary cyclic plasticity model	17
2.3.2 Stabilized or half-life based approximate cyclic plasticity model	18
2.4 Summary	21
3 Summary of Other Ongoing Experimental and Mechanistic Modeling Activities	22
3.1 Room temperature tensile and fatigue testing of 316 SS-316 SS similar metal weld specimens	22
3.2 Test set-up for elevated temperature tensile and fatigue testing	22
3.3 Cyclic plasticity model development for a realistic reactor component	23
3.4 Mechanistic model of welding process for further fatigue model development	24
4 Publication Activities	25

LIST OF FIGURES

Figure 2. 1 a) ANL’s in-air fatigue test set-up with capability to test both under room temperature and elevated temperature, b) typical hourglass specimen after fatigue tested, and c) the applied strain wave form used for the mentioned test. 3

Figure 2. 2 Overlapped hysteresis plot for $\epsilon_a^t = 0.25\%$ 4

Figure 2. 3 Magnified image of Figure 2.2 4

Figure 2. 4 Overlapped hysteresis plot for $\epsilon_a^t = 0.5\%$ 5

Figure 2. 5 Magnified image of Figure 2.4 5

Figure 2. 6 Overlapped hysteresis plot for $\epsilon_a^t = 0.75\%$ 6

Figure 2. 7 Magnified image of Figure 2.6 6

Figure 2. 8 Estimated upward and downward elastic modulus for $\epsilon_a^t = 0.25\%$ 7

Figure 2. 9 Estimated upward and downward elastic modulus for $\epsilon_a^t = 0.5\%$ 8

Figure 2. 10 Estimated upward and downward elastic modulus for $\epsilon_a^t = 0.75\%$ 8

Figure 2. 11 Evolution of maximum and minimum peak stress with respect to number of fatigue cycles for test cases $\epsilon_a^t = 0.25\%$, $\epsilon_a^t = 0.5\%$, and $\epsilon_a^t = 0.75\%$ 9

Figure 2. 12 Evolution of elastic strain range for test case $\epsilon_a^t = 0.25\%$ 10

Figure 2. 13 Evolution of plastic strain range for test case $\epsilon_a^t = 0.25\%$ 11

Figure 2. 14 Evolution of elastic strain range for test case $\epsilon_a^t = 0.5\%$ 11

Figure 2. 15 Evolution of plastic strain range for test case $\epsilon_a^t = 0.5\%$ 12

Figure 2. 16 Evolution of elastic strain range for test case $\epsilon_a^t = 0.75\%$ 12

Figure 2. 17 Evolution of plastic strain range for test case $\epsilon_a^t = 0.75\%$ 13

Figure 2. 18 Evolution of mean back stress for individual cycle (n) for test case $\epsilon_a^t = 0.25\%$ 14

Figure 2. 19 Evolution of mean back stress for individual cycle (n) for test case $\epsilon_a^t = 0.5\%$. 15

Figure 2. 20 Evolution of mean back stress for individual cycle (n) for test case $\epsilon_a^t = 0.75\%$ 15

Figure 2. 21 Evolution of plastic path travel based damage states (d_t) g for test cases $\epsilon_a^t = 0.25\%$, $\epsilon_a^t = 0.5\%$, and $\epsilon_a^t = 0.75\%$ 16

Figure 2. 22 Schematic showing relation between t and $t + \Delta t$ with respect to applied strain cycle 17

Figure 2. 23 Overlapping half-life hysteresis curves for test cases $\epsilon_a^t = 0.25\%$, $\epsilon_a^t = 0.5\%$,
and $\epsilon_a^t = 0.75\%$ and associated monotonic stress-strain curve 19

Figure 2. 24 Finite element model of the hourglass specimen shown in Figure 2.1 20

Figure 2. 25 Comparison of preliminary finite element estimated hysteresis curve with
experiment based half-life hysteresis curve for an applied strain amplitude of
 $\epsilon_a^t = 0.5\%$ 20

Figure 3. 1 Temperature profile measured from different thermocouples mounted on an
hourglass specimen and on pull rods of test frame. The higher temperature profiles
are around the gage length of the specimen. 22

Figure 3. 2 Preliminary results showing the stress distribution of a part-through cracked
surge-line pipe at the end of a single pressure cycle. 23

Figure 3. 3 Preliminary results showing the temperature distribution after few weld layers. .. 24

ABBREVIATIONS

ANL	Argonne National Laboratory
CF	Corrosion Fatigue
DOE	Department of Energy
FEM	Finite Element Method
LWR	Light Water Reactor
LWRS	Light Water Reactor Sustainability
NRC	Nuclear Regulatory Commission
RT	Room Temperature
SCC	Stress Corrosion Cracking
SS	Stainless Steel
XFEM	Extended Finite Element Method

ACKNOWLEDGMENTS

This research was sponsored by the U.S. Department of Energy, Office of Nuclear Energy, for the Light Water Reactor Sustainability Research and Development effort.

1 Introduction

Under the light water reactor sustainability (LWRS) program, the following two major activities are being conducted at Argonne National Laboratory:

- a) Mechanistic modeling of environmental fatigue for LWR piping materials
- b) Environmental tensile and/or fatigue testing of LWR pipe base, similar and dissimilar metal welds.

This quarterly report summarizes some of the work conducted from April – June 2013. During this period following tasks are performed

- Completion of room-temperature fatigue testing of four 316 SS base metal specimens. The resulting data sets were analyzed for cyclic plasticity constitutive model development.
- Room-temperature tensile testing of one 316 SS-316 SS similar metal weld specimen obtained from the fusion zone.
- Room-temperature fatigue testing of one 316 SS-316 SS similar metal weld specimen obtained from the fusion zone.
- Augmenting fatigue test set-up for elevated temperature testing.

The report is organized into two major sections such as:

Section 2 - Room-temperature fatigue test of 316 SS specimens and subsequent data analysis for cyclic plasticity constitutive model development

Section 3 - Ongoing experimental and mechanistic modeling activities

2 Room-Temperature Fatigue Test of 316 SS Specimens and Subsequent Data Analysis for Cyclic Plasticity Constitutive Model Development

2.1 Introduction

Mechanistic modeling of environmental fatigue requires developing various multi-physics finite element computer codes. Some of these are:

- a) Dynamic crack propagation modeling
- b) Cyclic plasticity and fatigue modeling
- c) Manufacturing process (e.g weld, forming, etc.) modeling
- d) Environmental effect modeling through coupled structural-multi-physics modeling

In our previous work (ANL/LWRS-13/1) we demonstrated the use of extended finite element method (XFEM) for dynamic crack propagation modeling. The next phase of the mechanistic modeling effort is to model cyclic plasticity. The cyclic plasticity modeling requires cyclic plasticity constitutive relations and related material properties. In the current reporting period, efforts were made to analyze the fatigue test data of 316 SS based metal specimens tested under in-air and room temperature conditions. Based on these data analysis, different types of cyclic plasticity models can be developed. These data analysis results and models are discussed below.

2.2 Fatigue testing of 316 SS base metal specimens and resulting data analysis

Four 316 SS hourglass specimens were fatigue tested in room-temperature air, one with 0.25% (F04), two with 0.5% (F01 and F02) and one with 0.75% (F03) strain amplitude using one of the ANL's fatigue test frame. The numbers within brackets denote the test sequence number or specimen numbers. All these tests were performed under strain control cycling with a strain rate of 0.001/s (0.1 %/s). Figure 2.1 shows the test frame, specimen (F02 after fatigue tested) and applied strain wave form. Note that, except specimen F01, all the other specimens were cycled until 25% peak load drop from the initial load. In contrast, specimen F01 was cycled until complete rupture. Also, since some discrepancies were observed during F01 specimen testing which are still being investigated, the related data are not discussed in this report. The details of the test data obtained from other three specimens fatigue testing are discussed below.

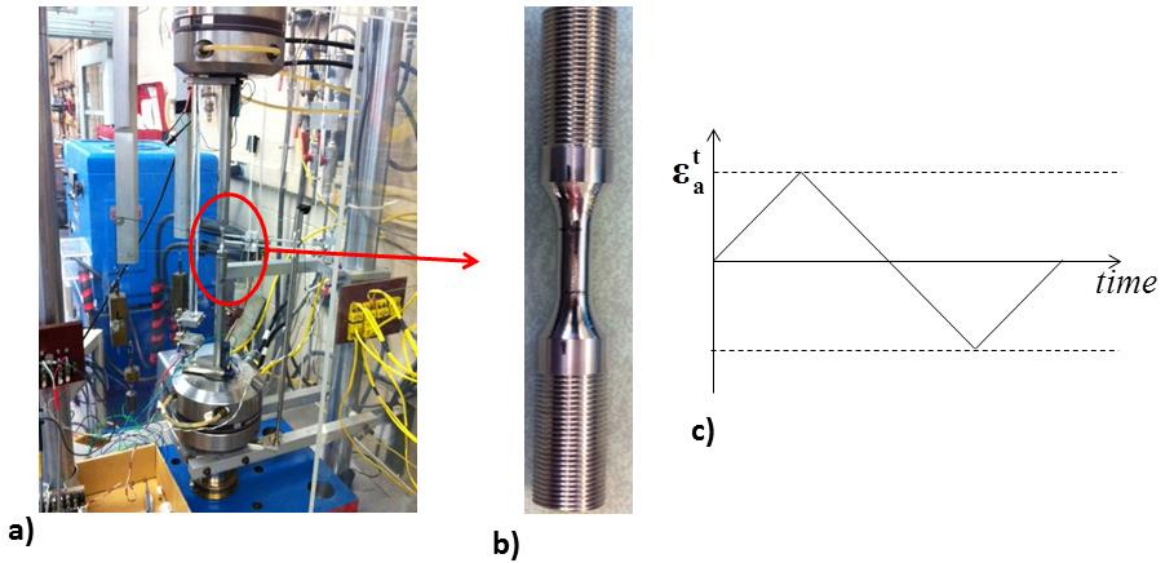


Figure 2. 1 a) ANL’s in-air fatigue test set-up with capability to test both under room temperature and elevated temperature, b) typical hourglass specimen after fatigue tested, and c) the applied strain wave form used for the mentioned test.

2.2.1 *Hysteresis behavior of 316SS base metal*

The evolution of the cyclic room-temperature hysteresis loops with time were recorded for the above mentioned tests ($\epsilon_a^t = 0.25\%$, $\epsilon_a^t = 0.5\%$, and $\epsilon_a^t = 0.75\%$). Figures 2.2, 2.4 and 2.6 show the overlapped cyclic stress-strain curves for $\epsilon_a^t = 0.25\%$, $\epsilon_a^t = 0.5\%$, and $\epsilon_a^t = 0.75\%$, respectively. From these figure it can be seen that after some initial hardening, the material softens. Also, the respective magnified hysteresis curves (refer to Figs. 2.3, 2.5, and 2.7) show that there are significant oscillations in the stress (e.g 60 MPa for $\epsilon_a^t = 0.25\%$ test) possibly due to dynamic strain aging. For accurate cyclic plasticity and hence fatigue life estimation it may be necessary to consider these oscillations in the stress.

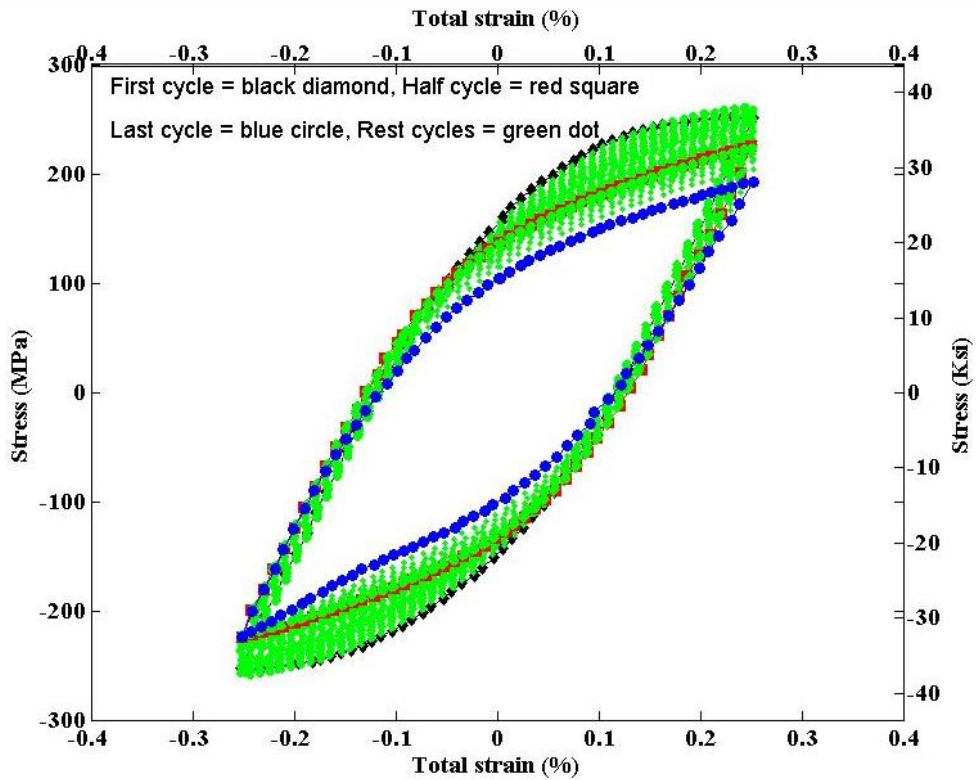


Figure 2. 2 Overlapped hysteresis plot for $\epsilon_a^t = 0.25\%$

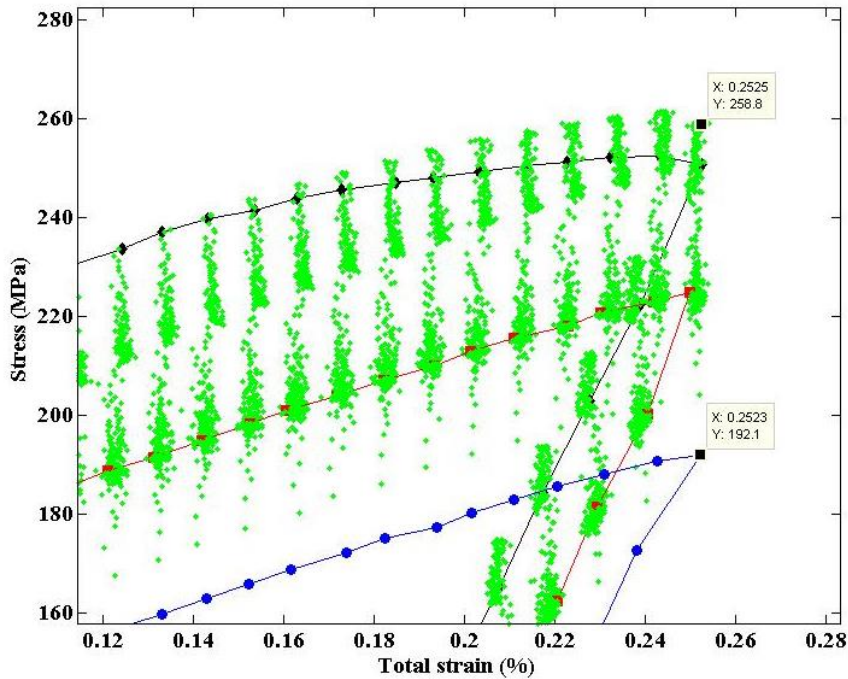


Figure 2. 3 Magnified image of Figure 2.2

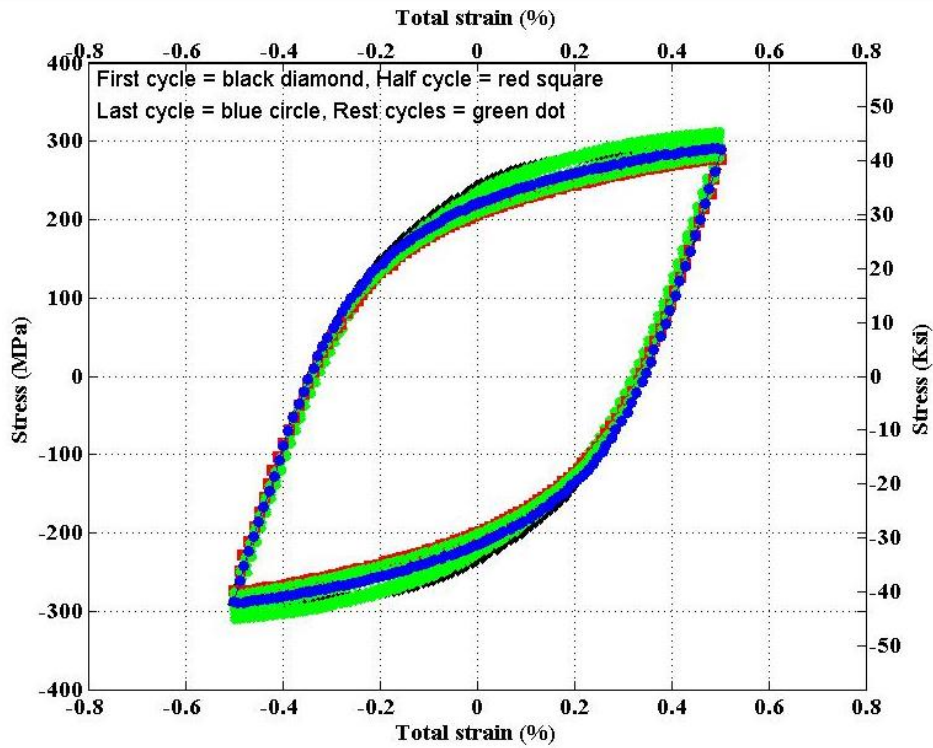


Figure 2.4 Overlapped hysteresis plot for $\epsilon_a^t = 0.5\%$

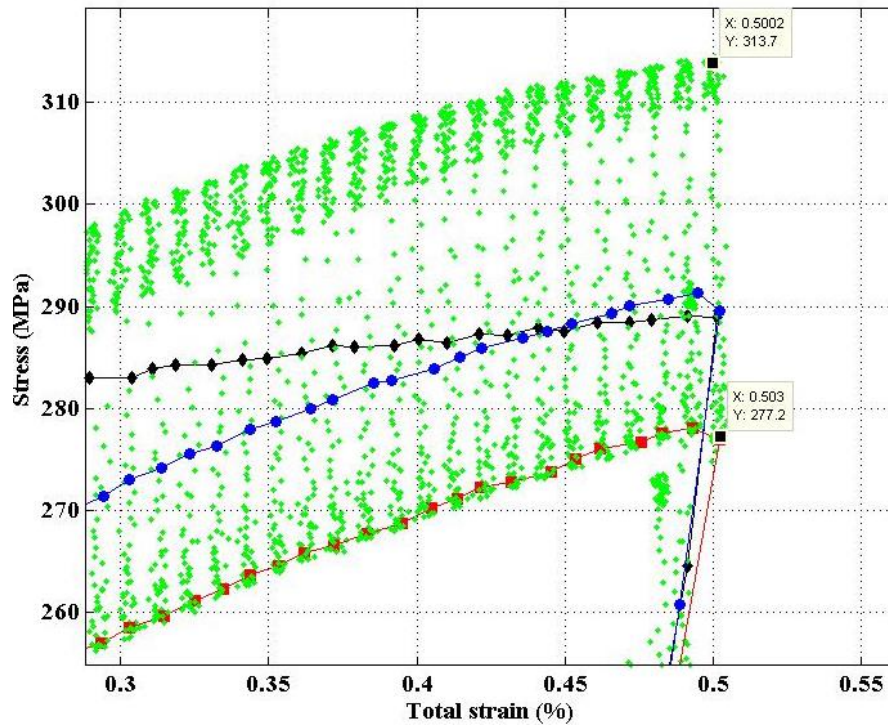


Figure 2.5 Magnified image of Figure 2.4

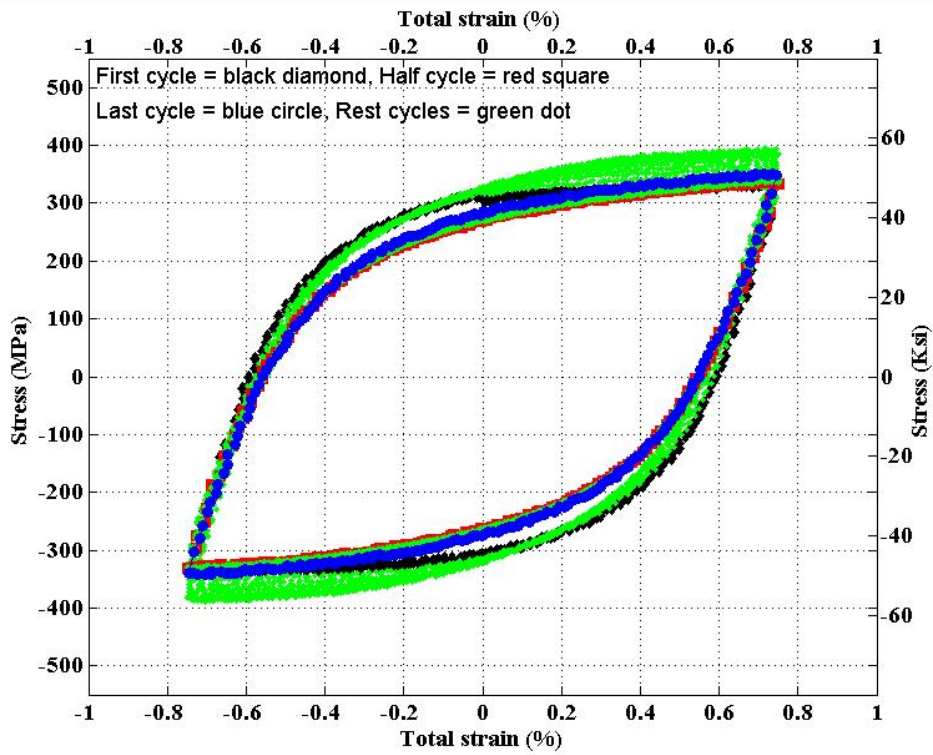


Figure 2. 6 Overlapped hysteresis plot for $\epsilon_a^t = 0.75\%$

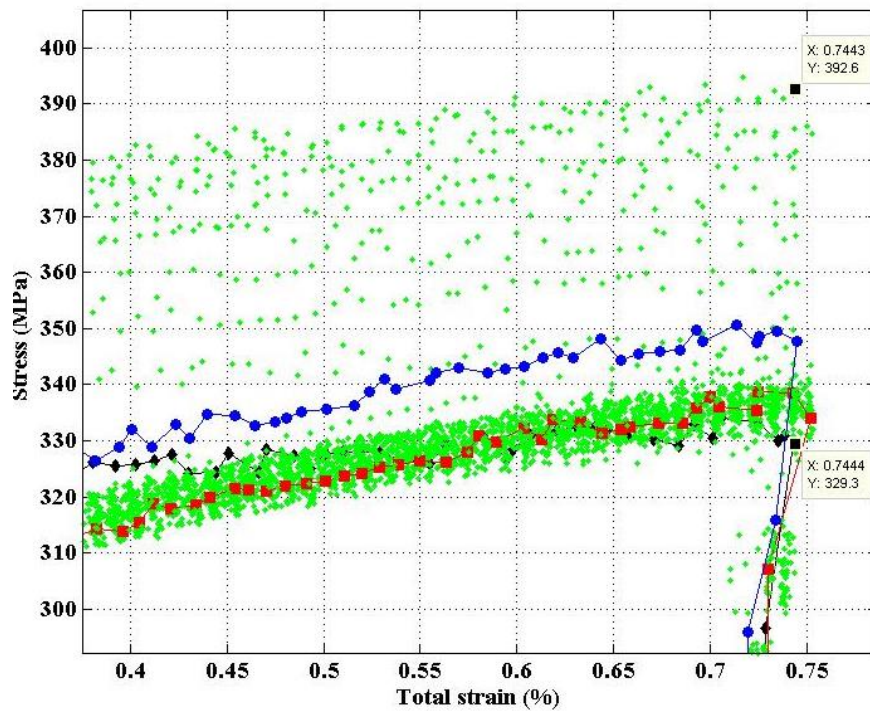


Figure 2. 7 Magnified image of Figure 2.6

2.2.2 Evolution of cyclic elastic modulus

To model cyclic plasticity it is also necessary to estimate cyclic elastic modulus and their evolution over time. For the mentioned tests we have also estimated both the upward and downward elastic modulus for individual cycles. Figures 2.8, 2.9 and 2.10 show the evolution of upward (E_{up}) and downward (E_{down}) moduli for the tests with $\epsilon_a^t = 0.25\%$, $\epsilon_a^t = 0.5\%$, and $\epsilon_a^t = 0.75\%$, respectively. From Fig. 2.8 it can be seen that for the test with $\epsilon_a^t = 0.25\%$, except during the end of the test, both elastic moduli vary between 180 to 190 GPa, with maximum variation within the range of 5-6%. It is to be noted that the monotonic elastic modulus for 316 SS estimated under similar conditions (e.g., under room temperature and with a strain rate of 0.1 %/Sec.) was 195.5 GPa (refer to ANL/LWRS-13/1). Similarly, from Fig. 2.9 it can be seen that for the test with $\epsilon_a^t = 0.5\%$, the elastic moduli vary in the range of 165-185MPa (10-12%). However, for $\epsilon_a^t = 0.75\%$, (refer Fig. 2.10) the elastic moduli varied in the range of 160-220 Mpa, which is more than 25-35%.

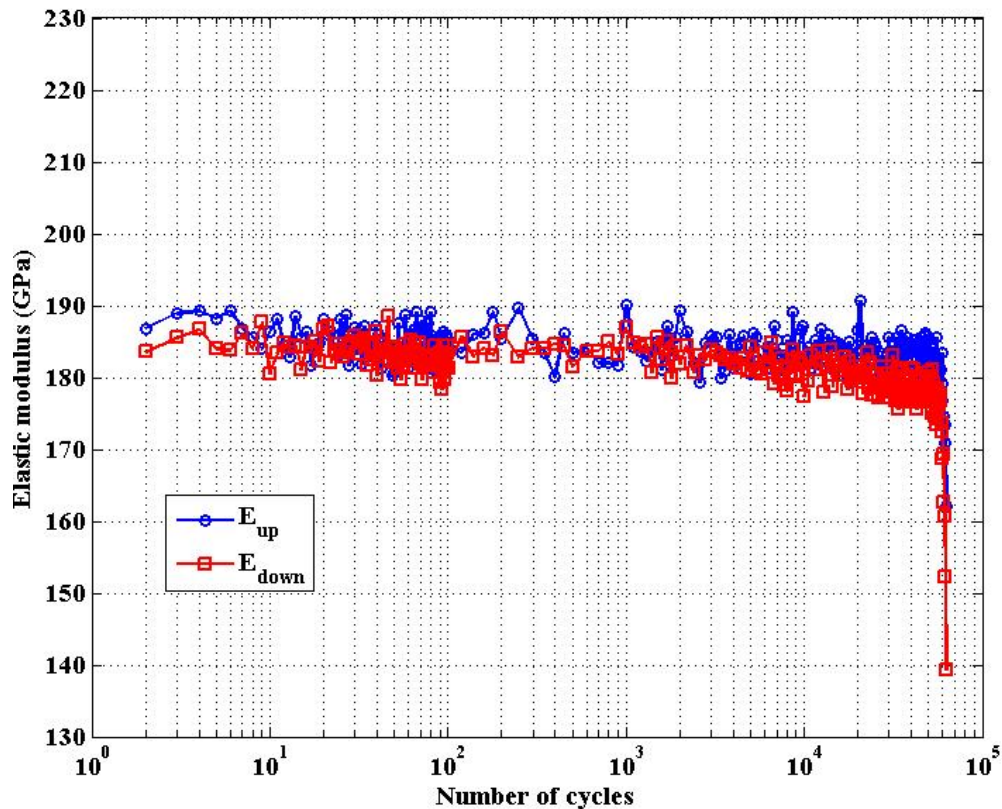


Figure 2. 8 Estimated upward and downward elastic modulus for $\epsilon_a^t = 0.25\%$

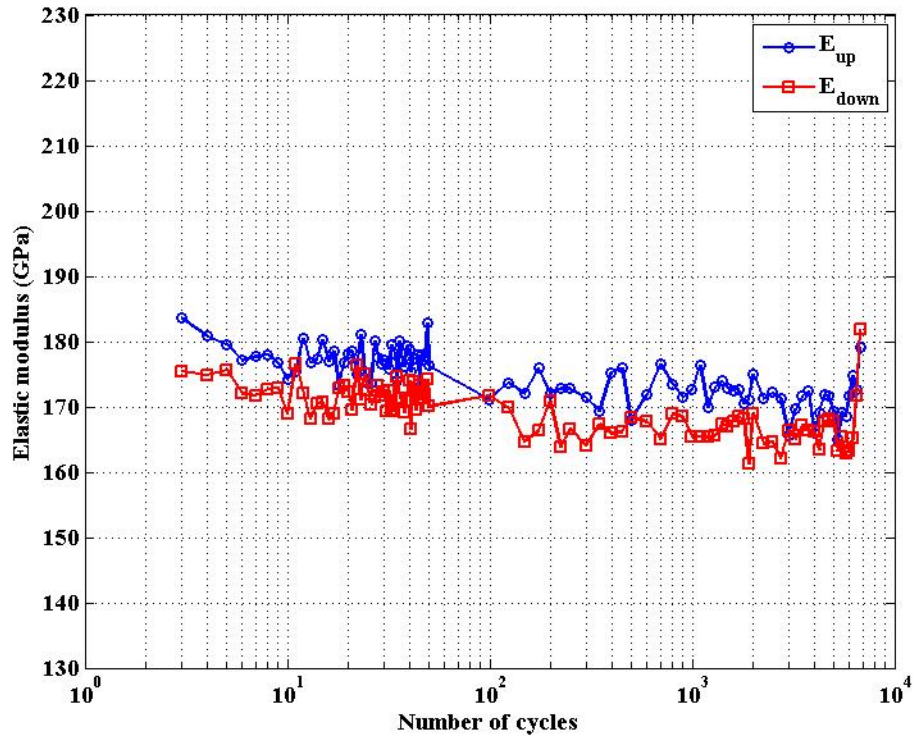


Figure 2. 9 Estimated upward and downward elastic modulus for $\epsilon'_a = 0.5\%$

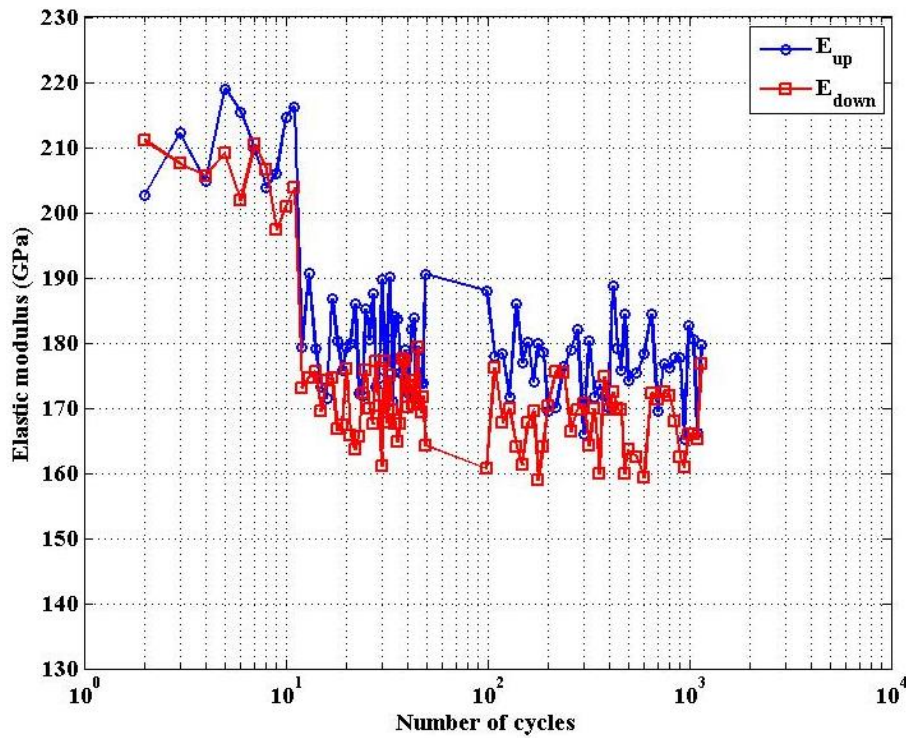


Figure 2. 10 Estimated upward and downward elastic modulus for $\epsilon'_a = 0.75\%$

2.2.3 Evolution of cyclic maximum (σ_n^{\max}) and minimum (σ_n^{\min}) peak stress

Different material can harden/soften differently depending on the applied stress/strain. Knowing the hardening and softening behavior of the material will help in developing suitable constitutive relationship for cyclic plasticity model. The evolution of hardening/softening behavior can be observed from the peak cyclic stress versus time or number of cycles curves. Figure 2.8 shows the evolution of peak maximum and minimum stresses for the tests with $\epsilon_a^t = 0.25\%$, $\epsilon_a^t = 0.5\%$, and $\epsilon_a^t = 0.75\%$, respectively. From the figure it can be observed that, in all cases, the material initially harden and then soften. Also, it can be seen that the magnitude of hardening-softening increases as the applied strain amplitude or range increases. It can be observed that for the test with $\epsilon_a^t = 0.75\%$ there is an abrupt drop in the peak stresses during the 10th and 11th cycle, possibly indicating buckling of the specimen or slippage of the extensometer.

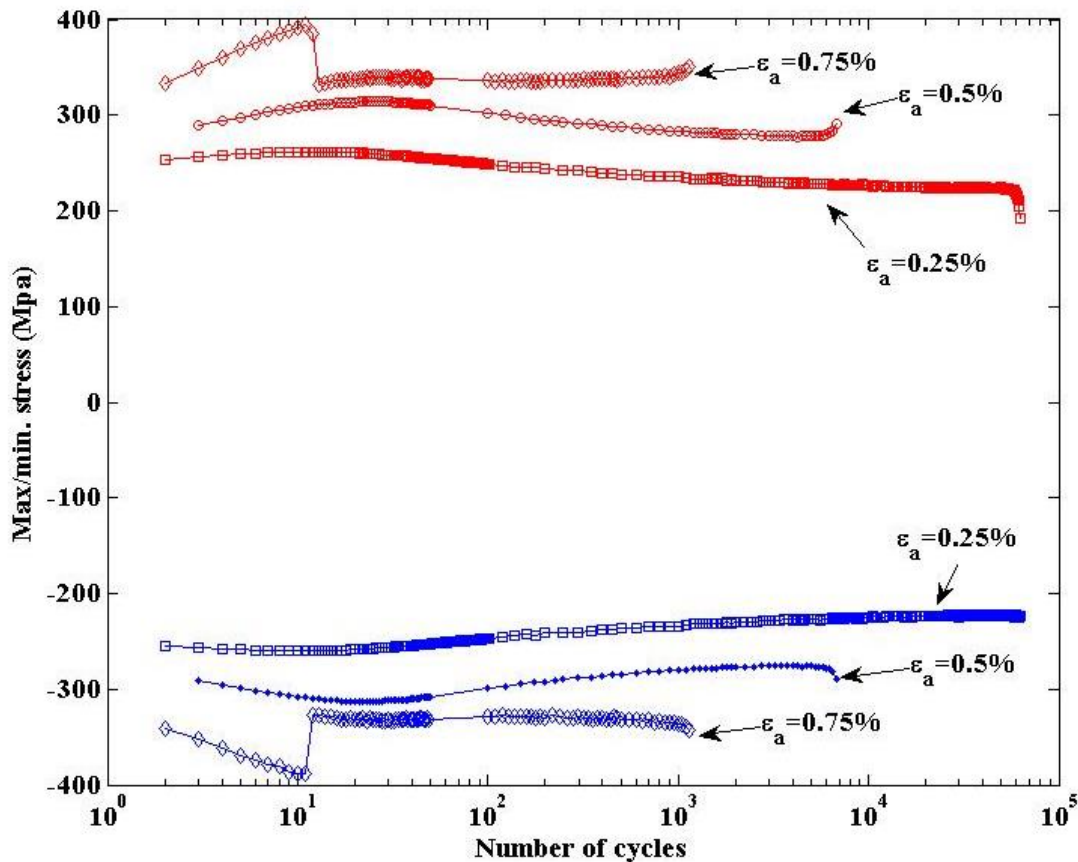


Figure 2.11 Evolution of maximum and minimum peak stress with respect to number of fatigue cycles for test cases $\epsilon_a^t = 0.25\%$, $\epsilon_a^t = 0.5\%$, and $\epsilon_a^t = 0.75\%$

2.2.4 Evolution of cyclic elastic strain range ($\Delta\varepsilon_n^e$) and plastic strain range ($\Delta\varepsilon_n^p$)

The variations of the elastic strain range ($\Delta\varepsilon_n^e$) and plastic strain range ($\Delta\varepsilon_n^p$) with number of fatigue cycle ($n=1, \dots, N$) are needed for development of the cyclic plasticity model. These trends can be linked to the cycle-dependent hardening and softening behavior of material, and will help us develop a suitable constitutive relation that can be incorporated to the mechanics based evolutionary cyclic plasticity model. Figures 2.12 and 2.13 show the variations of the elastic and plastic strain ranges with cycles for the test with $\varepsilon_a^t = 0.25\%$, respectively. Figures 2.14 and 2.15 show the corresponding evolutions for the test with $\varepsilon_a^t = 0.5\%$ and Figs 2.16 and 2.17 show the evolutions for the test with $\varepsilon_a^t = 0.75\%$, respectively. From these figures it can be observed that, except for the test with $\varepsilon_a^t = 0.75\%$ (Figures 2.16 and 2.17), similar trends in elastic and plastic strain range evolution are observed for tests with $\varepsilon_a^t = 0.25\%$ and $\varepsilon_a^t = 0.5\%$. For example, Fig. 2.12 shows that the elastic strain range ($\Delta\varepsilon_n^e$) initially increases and then decreases, which indicates initial hardening followed by softening. Figure 2.13 shows that the plastic strain range ($\Delta\varepsilon_n^p$) initially decreases and then increases, which also indicates initial hardening and then softening. The continuous hardening with cycle in the case of $\varepsilon_a^t = 0.75\%$ is possibly due to the large applied strain amplitude indicating a trend towards stress saturation and a stable hysteresis loop. However, the possibility of buckling makes this test questionable.

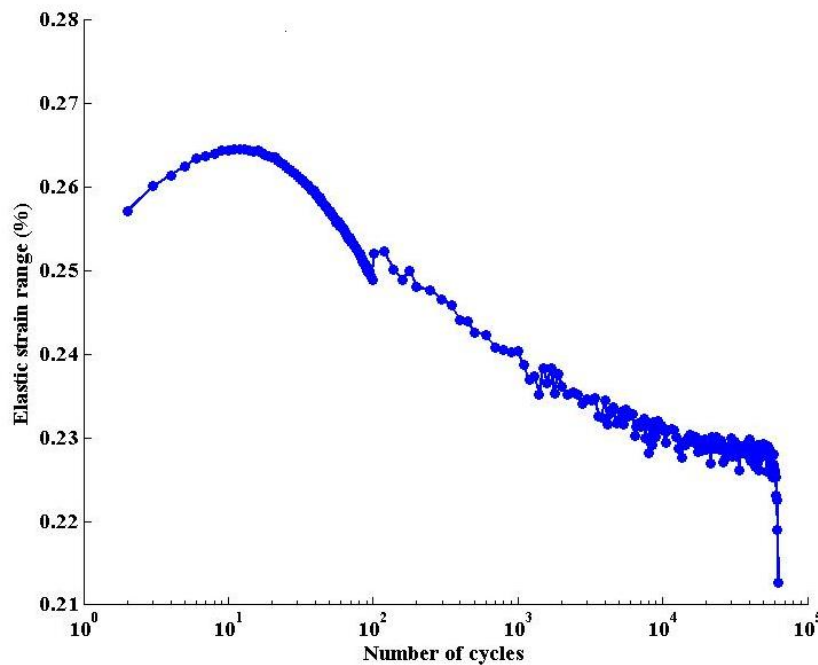


Figure 2.12 Evolution of elastic strain range for test case $\varepsilon_a^t = 0.25\%$

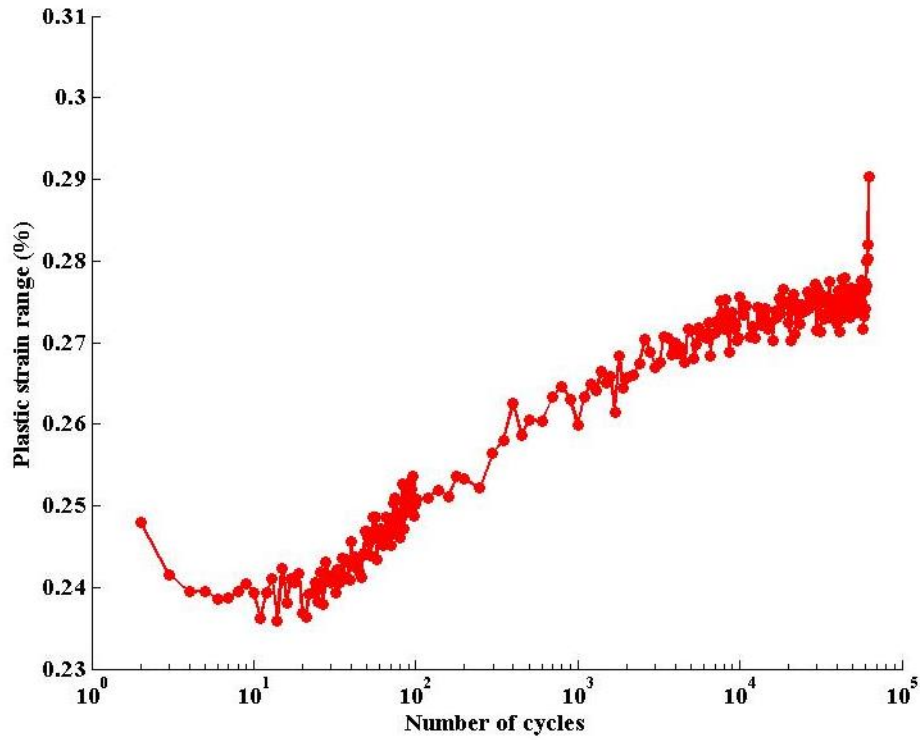


Figure 2. 13 Evolution of plastic strain range for test case $\varepsilon_a^t = 0.25\%$

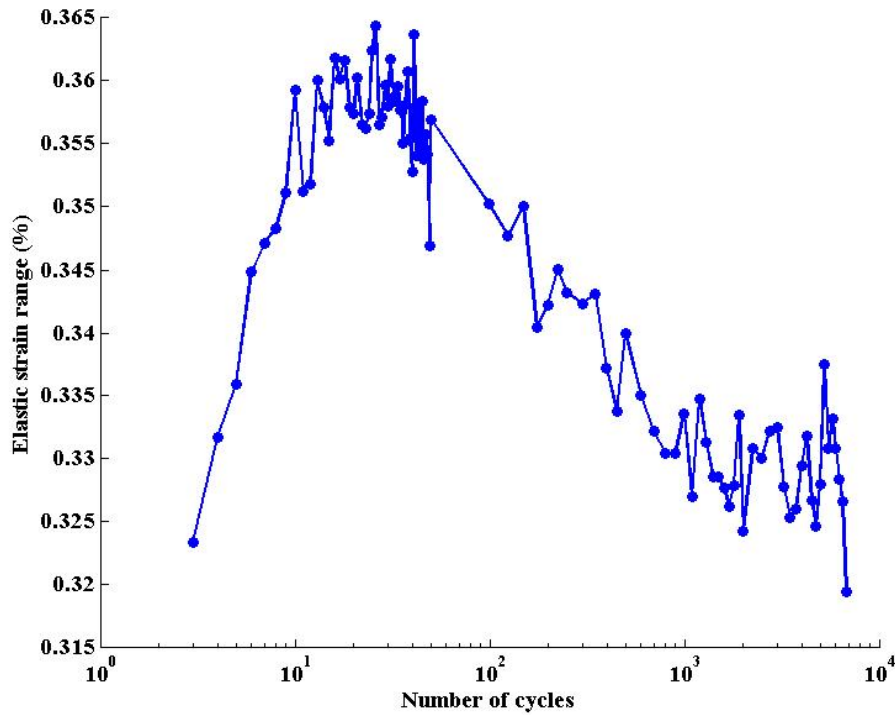


Figure 2. 14 Evolution of elastic strain range for test case $\varepsilon_a^t = 0.5\%$

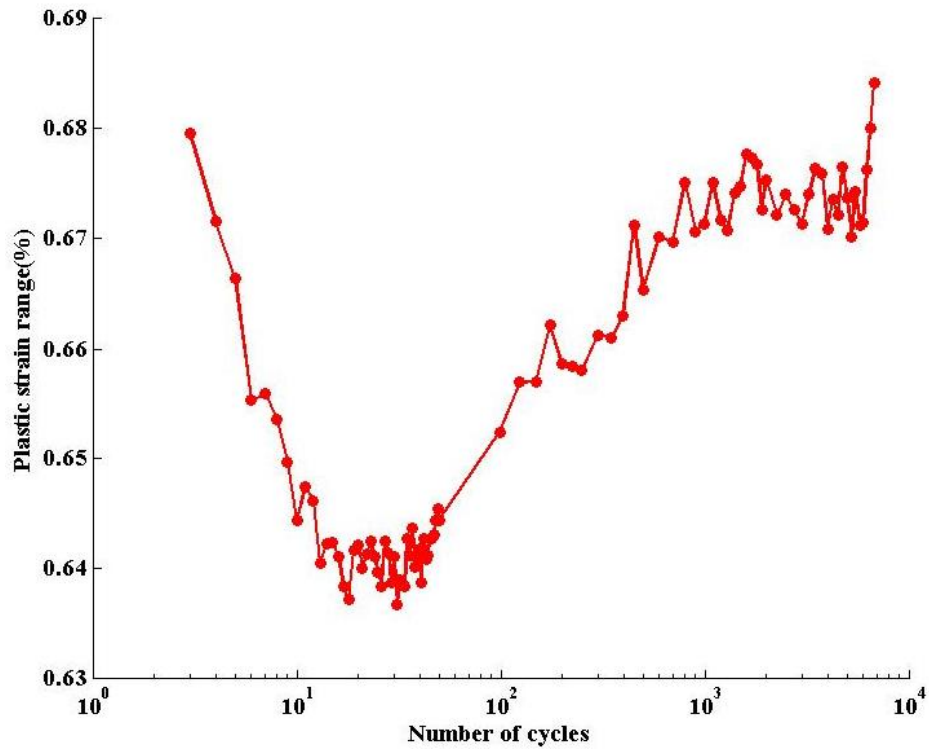


Figure 2. 15 Evolution of plastic strain range for test case $\varepsilon_a^t = 0.5\%$

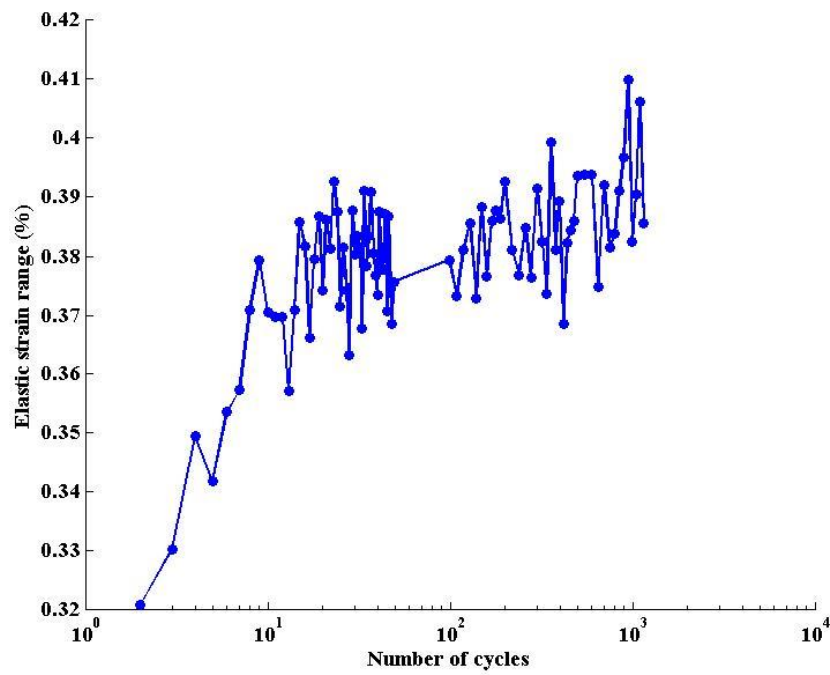


Figure 2. 16 Evolution of elastic strain range for test case $\varepsilon_a^t = 0.75\%$

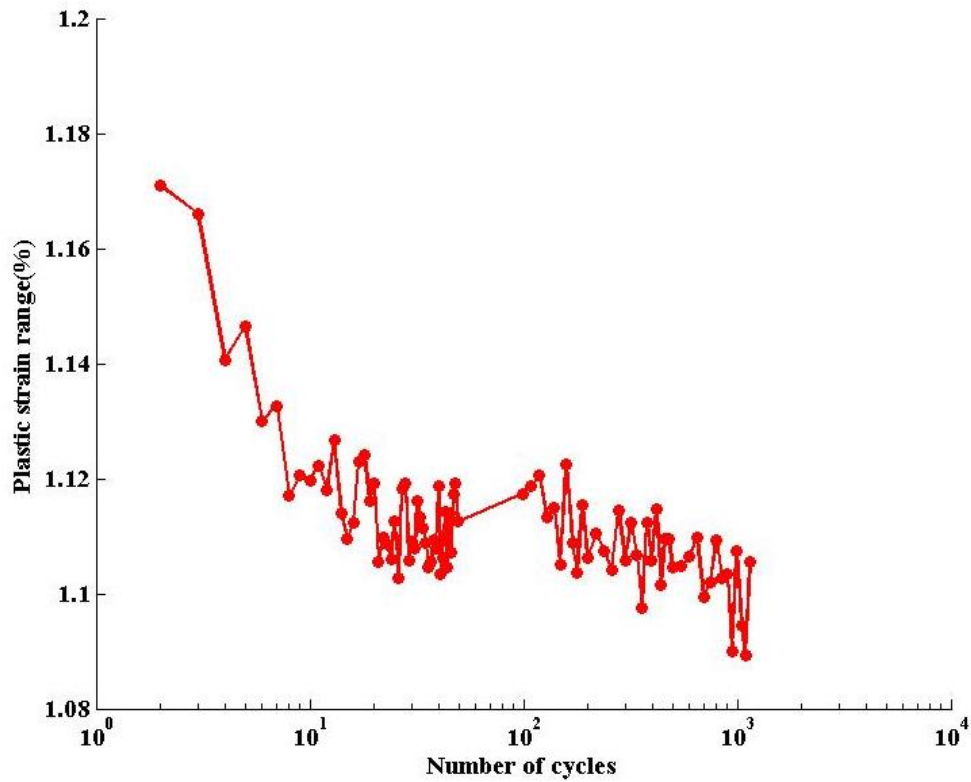


Figure 2.17 Evolution of plastic strain range for test case $\varepsilon_a^t = 0.75\%$

2.2.5 Evolution of cyclic back stress (α_t)

When there is a stress reversal, the hysteresis loop moves up or down from its original position depending on the material and applied stress/strain. This is due to strain hardening/softening and associated Bauschinger effect. This shift in stress space can be represented by a back stress (α_t). The estimation of evolution of back stress with respect to time is necessary for modeling cyclic plasticity. The evolution of back stress α_t at any given instant of time can be expressed as:

$$\alpha_t = \alpha_n + \alpha_\varepsilon \quad (2.1)$$

Where, α_n is the mean shift of hysteresis loop in stress space and can be expressed as

$$\alpha_n = \frac{1}{2} (\sigma_{n;\varepsilon=\varepsilon_{\max}}^t + \sigma_{n;\varepsilon=\varepsilon_{\min}}^c) \quad (2.2)$$

and α_ε is the back stress at strain ε within an individual hysteresis loop and can be expressed as

$$\alpha_n = \frac{1}{2}(\sigma_{n;\varepsilon}^{ten} + \sigma_{n;\varepsilon}^{com}) \quad (2.3)$$

In Eq. 2.2 $\sigma_{n;\varepsilon=\varepsilon_{max}}^{ten}$ and $\sigma_{n;\varepsilon=\varepsilon_{min}}^{com}$ denote the n^{th} fatigue cycle maximum tensile stress at $\varepsilon = \varepsilon_{max}$ and maximum compressive stress at $\varepsilon = \varepsilon_{min}$, respectively. For the tests with $\varepsilon_a^t = 0.25\%$, $\varepsilon_a^t = 0.5\%$, and $\varepsilon_a^t = 0.75\%$, the mean back stresses α_n were estimated and their evolutions are plotted in Figs 2.18, 2.19 and 2.20, respectively.

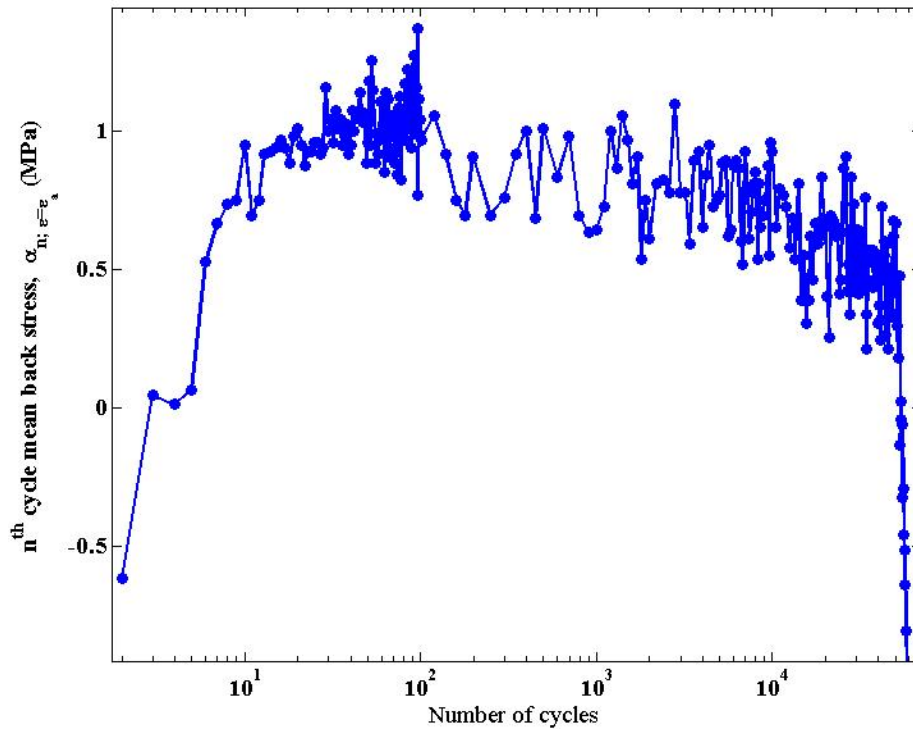


Figure 2. 18 Evolution of mean back stress for individual cycle (n) for test case $\varepsilon_a^t = 0.25\%$

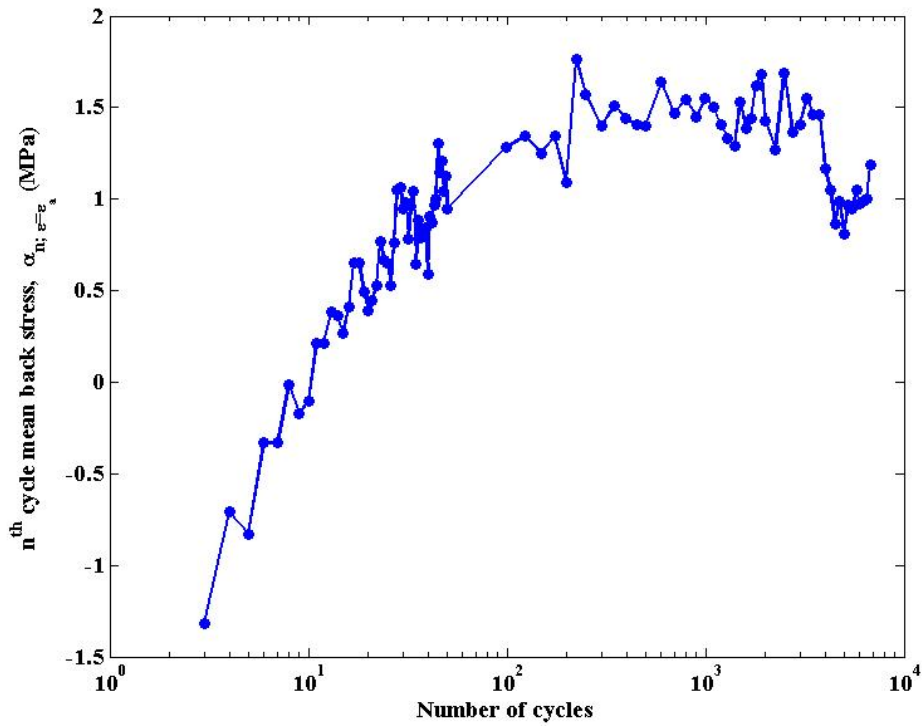


Figure 2. 19 Evolution of mean back stress for individual cycle (n) for test case $\varepsilon'_a = 0.5\%$

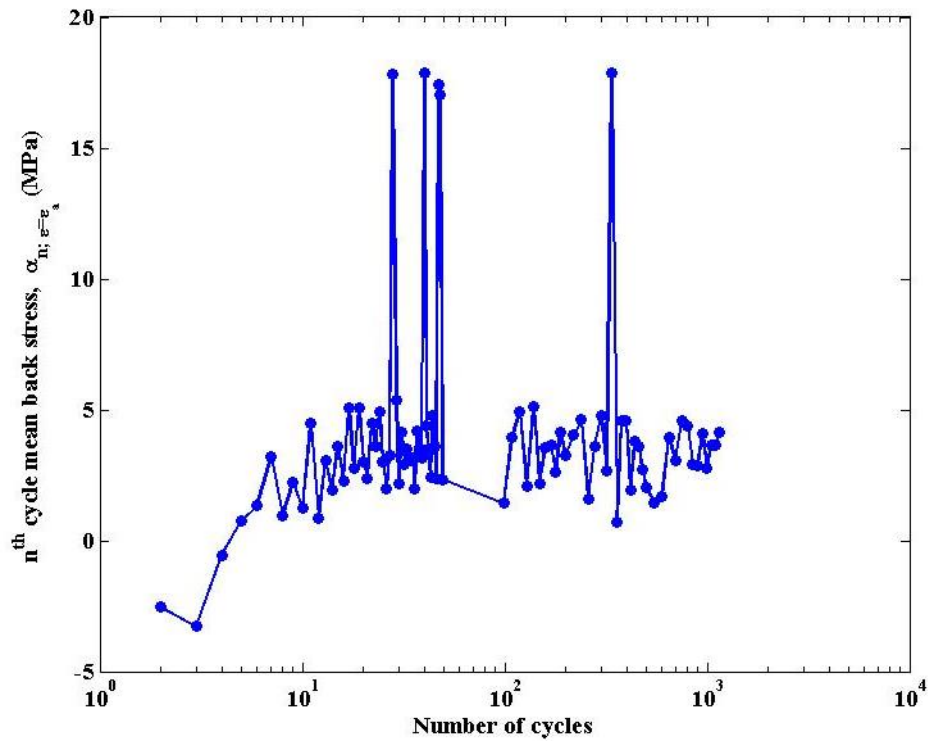


Figure 2. 20 Evolution of mean back stress for individual cycle (n) for test case $\varepsilon'_a = 0.75\%$

2.2.6 Evolution of damage state (d_t)

It may be necessary to associate the evolutionary stress-strain properties to a physical damage quantity say d_t . If so, in the constitutive model for cyclic plasticity, the stress-strain relation properties can be input as a function of this time independent variable rather than explicitly expressing the material properties with respect to time. Though in a stress controlled fatigue test it may be easier to express d_t as function of accumulated plastic strain, it may not be straight forward in case of strain controlled fatigue tests. For example in strain controlled fatigue tests the damage state at any given instant of time d_t can be expressed in terms of accumulated plastic path length and is as given below:

$$d_t = P_p = \int d\varepsilon^p = 2 \sum_{n=1}^N \Delta\varepsilon_n^p \quad (2.4)$$

Figure 2.21 shows the corresponding estimated damage states for test cases $\varepsilon_a^t = 0.25\%$, $\varepsilon_a^t = 0.5\%$, and $\varepsilon_a^t = 0.75\%$, respectively. However, from the figure it can be seen that the estimated damage states are not truly cycle independent rather depends on the number of fatigue cycles the specimen experienced. This drawback may necessitate the need of performing few stress controlled fatigue tests at least for developing evolutionary plasticity and hence the evolutionary fatigue model.

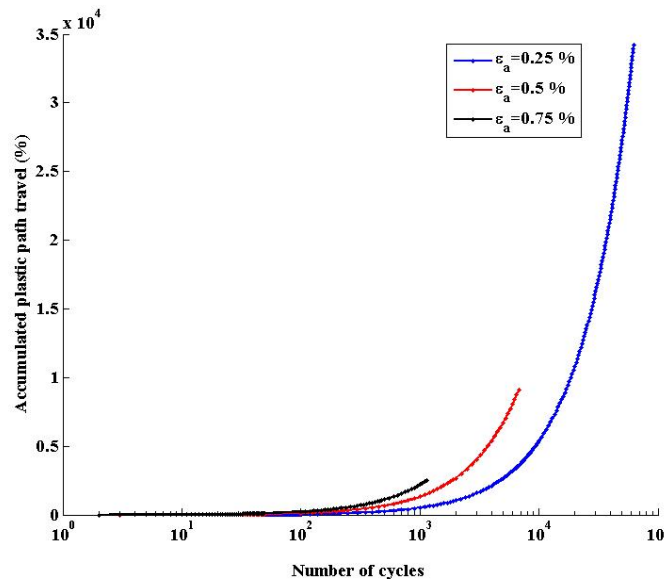


Figure 2. 21 Evolution of plastic path travel based damage states (d_t) g for test cases $\varepsilon_a^t = 0.25\%$, $\varepsilon_a^t = 0.5\%$, and $\varepsilon_a^t = 0.75\%$

2.3 Constitutive model for cyclic plasticity

The constitutive relation for the cyclic plasticity model can be developed based on the above discussed test results. The constitutive relation can be of two types such as evolutionary cyclic plasticity model and stabilized or half-life based cyclic plasticity model. Both these models are discussed briefly below.

2.3.1 Detailed evolutionary cyclic plasticity model

The evolutionary plasticity model captures the evolution of material parameters over the entire fatigue life. To apply this model, the material parameters such as elastic modulus, yield stress, elastic strain range, plastic strain range, back stress, hardening constants, etc. have to be described as functions of time independent parameter(s) describing the physical damage state of the structure. For example, the stress state at time $t + \Delta t$ can be expressed as

$$\begin{aligned}\sigma_{t+\Delta t} &= \sigma_t + \Delta\sigma \\ \Delta\sigma &= C : \Delta\varepsilon^{el} = C : (\Delta\varepsilon^{to} - \Delta\varepsilon^{pl})\end{aligned}\quad (2.4)$$

Where C is the elasticity matrix, σ_t is the stress up to time t and can be expressed in terms of stress up to n^{th} fatigue cycle using the following relation;

$$\sigma_t = \sigma_n + \sigma_{\bar{t}} \quad (2.5)$$

Where the time equivalent of n^{th} fatigue cycle is equal to nT where T is the time period of an individual fatigue cycle and \bar{t} is elapsed time in an individual cycle. The relationship between \bar{t} and $t + \Delta t$ is schematically shown in Figure 2.22.

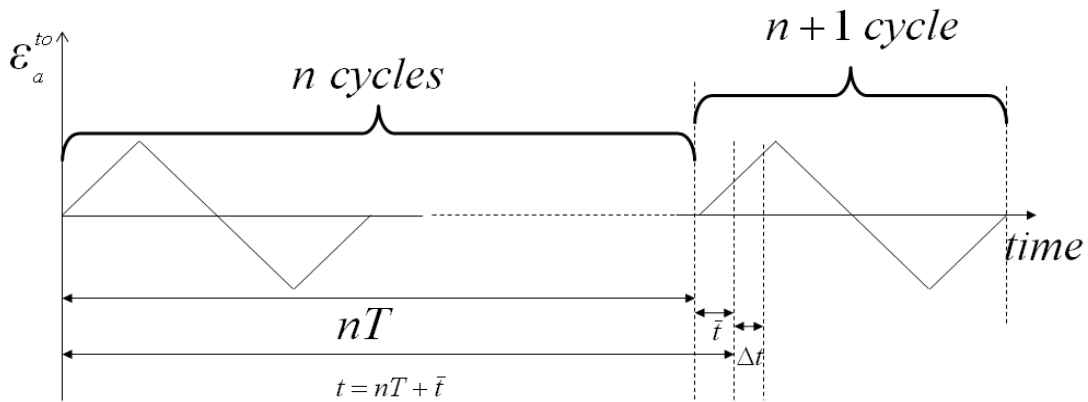


Figure 2.22 Schematic showing relation between \bar{t} and $t + \Delta t$ with respect to applied strain cycle

In Eq. 2.4, $\sigma_{t+\Delta t}$ is the true stress estimated from a two-step process, first by estimating a trial stress ${}^{trial}\sigma_{t+\Delta t}$ in solving Eq. 2.4 with the assumption of $\Delta\varepsilon^{pl} = 0$ (elastic predictor step) and then correcting the trial stress by satisfying the Von-mises yield criteria (plastic corrector step) given as

$$f = ({}^{trial}\sigma'_{t+\Delta t} - \alpha_{t+\Delta t}) : ({}^{trial}\sigma'_{t+\Delta t} - \alpha_{t+\Delta t}) - \sigma_{t+\Delta t}^y = 0 \quad (2.6)$$

Where ${}^{trial}\sigma'_{t+\Delta t}$ is the trial deviatoric stress tensor, $\alpha_{t+\Delta t}$ is the back stress tensor at time $t + \Delta t$ and can be expressed as

$$\alpha_{t+\Delta t} = \alpha_n + \alpha_{\bar{t}+\Delta t} \quad (2.7)$$

Where, α_n is the evolutionary contribution expressed as a function of cycles and $\alpha_{\bar{t}+\Delta t}$ is the contribution within a particular cycle expressed as a function of time. The evolutionary contribution corrects the $\alpha_{\bar{t}+\Delta t}$ by considering the evolutionary effect of stress hardening and softening. Similarly in Eq.2.6, the yield stress $\sigma_{t+\Delta t}^y$ can also be expressed in terms of a correction part (σ_n^y) which is a function of cycles and a yield stress ($\sigma_{\bar{t}+\Delta t}^y$) within an individual cycle which is a function of time as follows:

$$\sigma_{t+\Delta t}^y = \sigma_n^y + \sigma_{\bar{t}+\Delta t}^y \quad (2.8)$$

The cycle-dependent correction α_n for back stress and σ_n^y for yield stress have to be related to a time or cycle independent physical parameters (e.g accumulated plastic strain in a stress controlled test).

2.3.2 Stabilized or half-life based approximate cyclic plasticity model

Typically estimating the evolutionary correction terms described through Eq. 2.7 and 2.8 are highly complex and requires multiple fatigue test data sets to estimate the general trend and associated non-linear relationships with other independent variables. Hence for simplicity in the present work the evolutionary correction terms in Eq. 2.7 and 2.8 are not considered. In addition, to estimate the hardening and yield parameter only the half-life hysteresis curves of all the three tests with $\varepsilon_a^t = 0.25\%$, $\varepsilon_a^t = 0.5\%$, and $\varepsilon_a^t = 0.75\%$ are considered. A cyclic stress-strain curve is estimated by connecting the peak maximum stress point of the individual plastic strain versus stress hysteresis curves. Figure 2.23 shows the half-life hysteresis curve of the individual test cases and the associated tensile half of the cyclic stress-strain curve. In a similar fashion, the compressive half of the cyclic stress-strain curve can be estimated by connecting the peak

minimum stress point of the individual plastic strain versus stress hysteresis curves. From Fig. 2.23 it can be seen that both the tensile and compressive halves of the cyclic stress-strain curve follow a linear pattern and the corresponding hardening parameter are estimated by directly estimating the slopes of these linear stress-strain curves and the yield stress as the corresponding y-intercepts. Because of lack of data, the usual 0.2% offset strain is not determined in this case. A stabilized or half-life cyclic stress-strain curve can be constructed by performing a number of strain-controlled fatigue tests at different strain amplitudes. The same information can be obtained by performing a single strain controlled fatigue tests with a sequence of different strain amplitudes, which are repeated at certain regular intervals. The hardening parameters can be estimated from the estimated cyclic stress-strain curve. For example, the tensile hardening constant is estimated as 24.426 GPa and the corresponding yield stress as 194 MPa. The respective compressive hardening constant and yield stress are found to be 24.183 GPa and 194 MPa, respectively. It is noted that the monotonic yield stress estimated from monotonic tensile tests under similar test conditions (e.g room temperature, strain rate = 0.1%/Sec.) was 245.3 MPa (refer to ANL/LWRS-13/1). Based on the above mentioned cyclic yield stress and hardening parameters a preliminary finite element model of the fatigue specimen (refer Figure 2.1) was developed (Fig. 2.24). Figure 2.25 shows a comparison of the hysteresis loop calculated by the finite element model with the experimentally determined hysteresis loop. It can be seen that the two hysteresis loops are qualitatively similar. The finite element model was developed using ABAQUS software and assuming linear kinematic hardening condition.

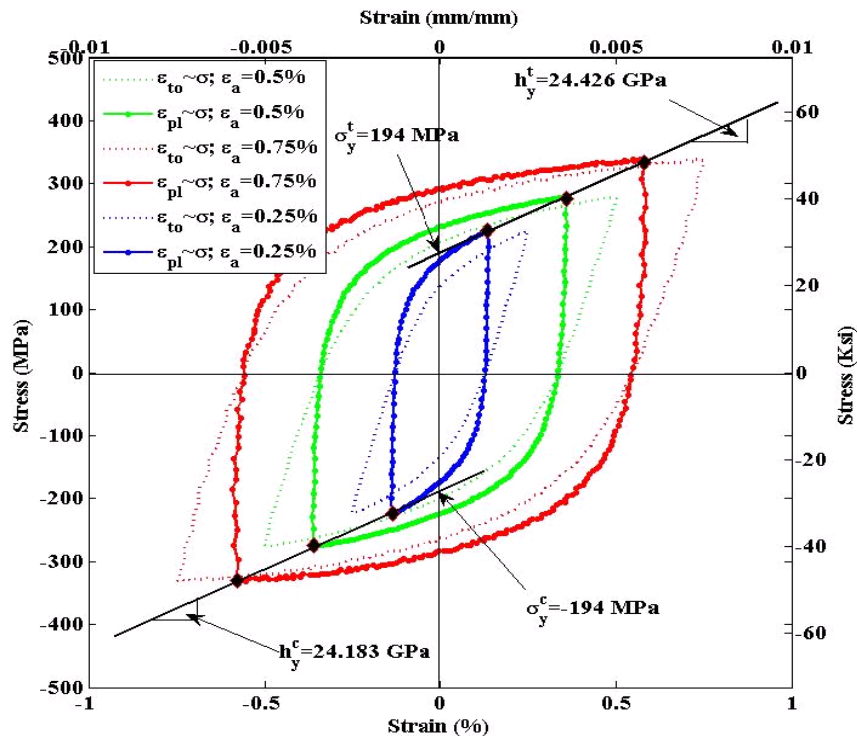


Figure 2. 23 Overlapping half-life hysteresis curves for test cases $\epsilon_a^t = 0.25\%$, $\epsilon_a^t = 0.5\%$, and $\epsilon_a^t = 0.75\%$ and associated monotonic stress-strain curve

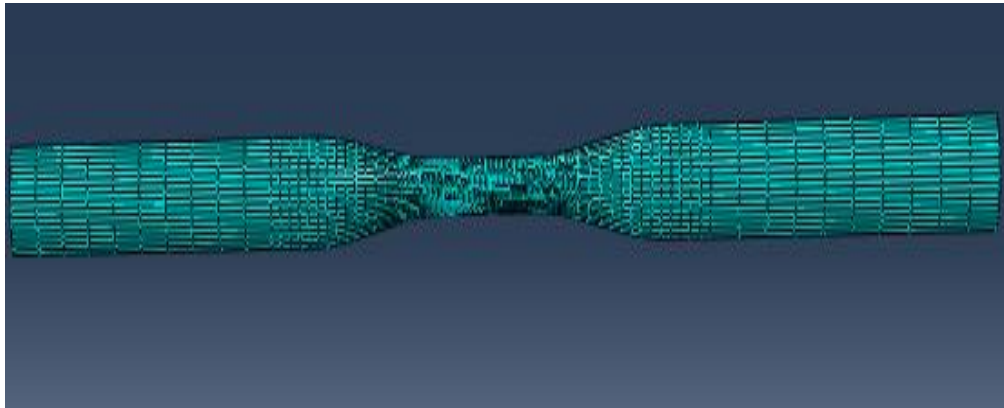


Figure 2. 24 Finite element model of the hourglass specimen shown in Figure 2.1

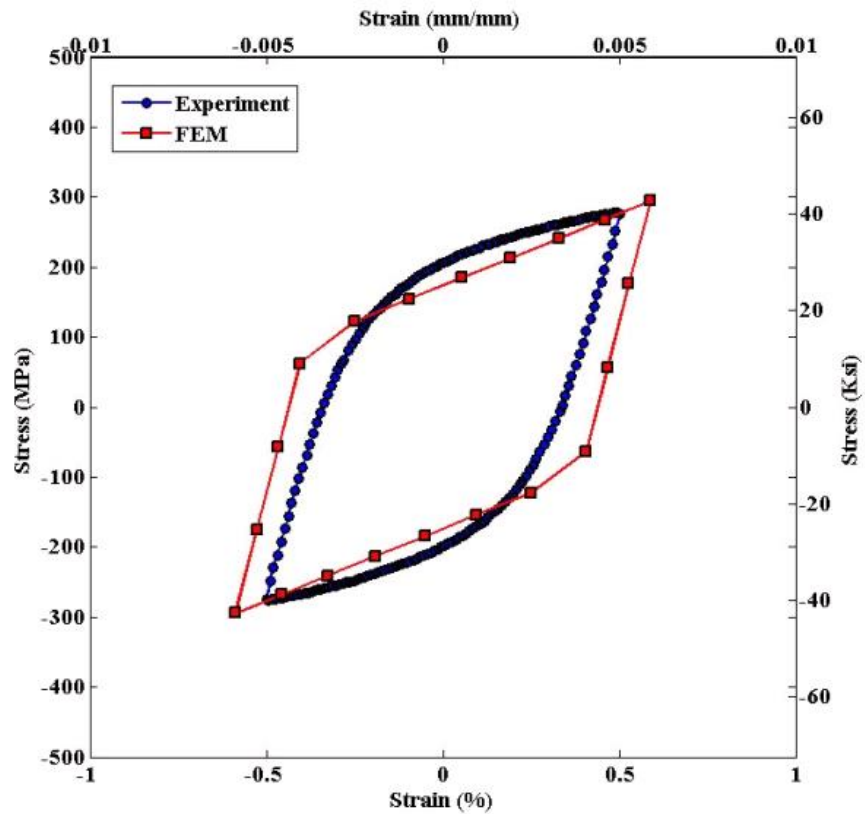


Figure 2. 25 Comparison of preliminary finite element estimated hysteresis curve with experiment based half-life hysteresis curve for an applied strain amplitude of $\epsilon_a^t = 0.5\%$

2.4 Summary

The room temperature fatigue test data of 316SS base metal specimen are analyzed to derive the hardening and softening behavior of 316SS base metal under in-air and room temperature conditions. This analysis will help develop a suitable constitutive relation for a mechanistically based cyclic plasticity or fatigue model. In addition, the information obtained through this test data will help us plan the next series of tests, such as, elevated temperature and water environment fatigue testing of base and weld specimens. Both evolutionary plasticity model and half-life hysteresis loop based approximate cyclic plasticity models are discussed. Based on half-life cycle hysteresis curves, a cyclic stress-strain curve was estimated which together with the assumption of linear kinematic hardening was used in a preliminary finite element analysis of the test specimen. The finite element model results were qualitatively similar to the experiment results. Based on the discussed room temperature fatigue test data, the FE model can be further improved, which is one of our future tasks.

3 Summary of Other Ongoing Experimental and Mechanistic Modeling Activities

During the reporting period following works are finished or continued under the LWRS environmental fatigue task.

3.1 Room temperature tensile and fatigue testing of 316 SS-316 SS similar metal weld specimens

- a) One room temperature tensile testing of 316SS similar metal weld specimen conducted with a strain rate of 0.001 /S (0.1 % /S). The specimen was obtained from the fusion zone.
- b) One room temperature fatigue testing of 316SS similar metal weld specimen conducted with a strain amplitude of 0.6 % and strain rate of 0.001 /S (0.1 % /S). The specimen was obtained from the fusion zone.

3.2 Test set-up for elevated temperature tensile and fatigue testing

The fatigue test set-up used for the room-temperature fatigue testing (refer Figure 2.1) discussed in section 2 is being augmented with a heating source for elevated temperature fatigue testing. Figure 3.1 shows the temperature measurements from various thermocouples mounted on the pull rod and specimen.

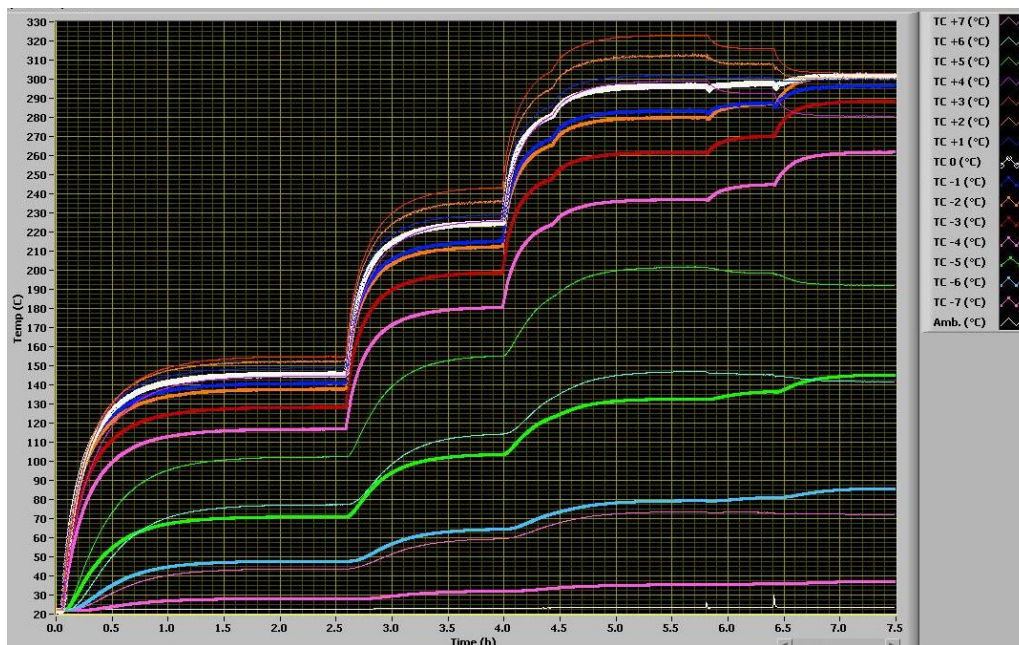


Figure 3. 1 Temperature profile measured from different thermocouples mounted on an hourglass specimen and on pull rods of test frame. The higher temperature profiles are around the gage length of the specimen.

3.3 Cyclic plasticity model development for a realistic reactor component

The finite element based cyclic plasticity model discussed in section 2 is being further improved to incorporate nonlinear kinematic hardening. Also the FE model discussed in section 2 is based on hourglass type specimen. In general, this type of specimen experiences uniaxial stress profile across the gage area. However, realistic component experiences multi-axial loading. Hence to accurately estimate the fatigue life of reactor components it is necessary to develop the cyclic plasticity model using realistic reactor component geometry. Figure 3.2 shows the preliminary finite model of a surge line pipe with a pre-existing crack.

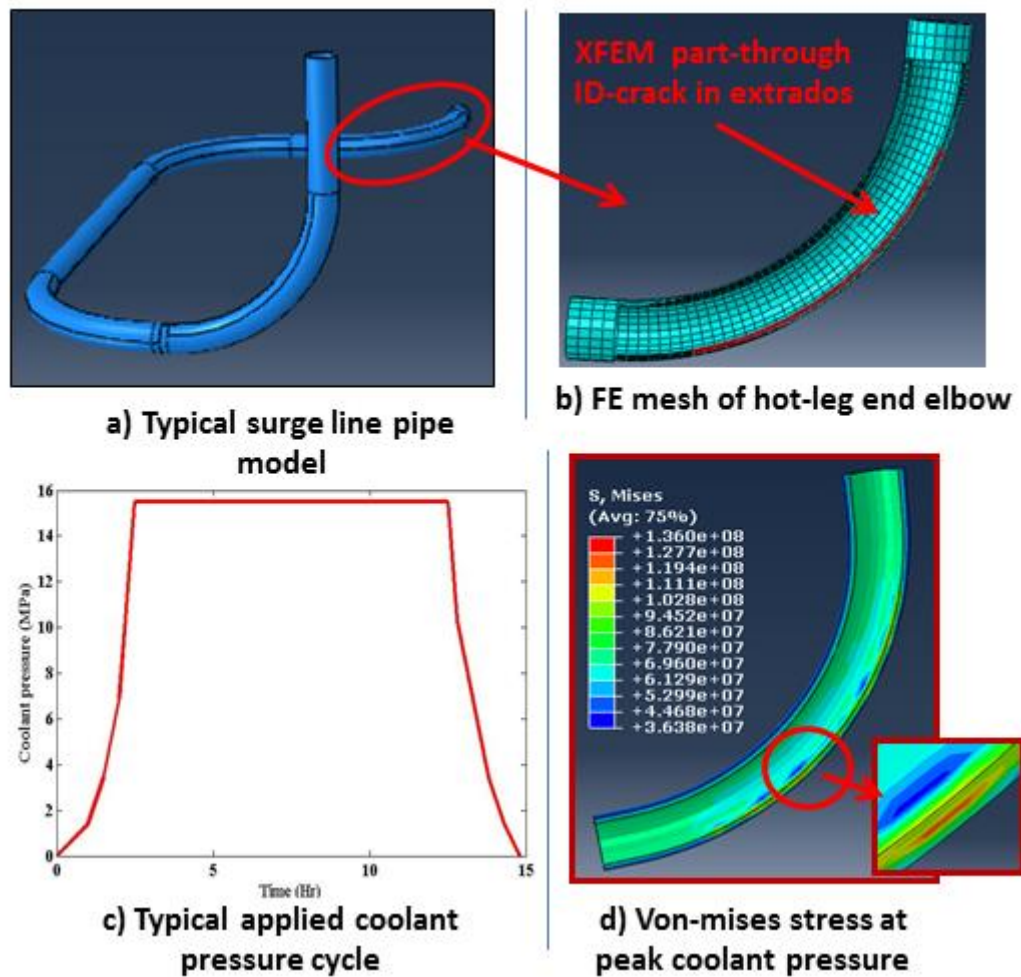


Figure 3. 2 Preliminary results showing the stress distribution of a part-through cracked surge-line pipe at the end of a single pressure cycle.

3.4 Mechanistic model of welding process for further fatigue model development

To develop a mechanics based environmental fatigue mode of a welded component/specimen, it is necessary to include the residual stresses that would be generated by the welding process in the fatigue model. Efforts are being made to model the weld process through finite element model. Figure 3.3 show the example of preliminary FE model results (temperature distribution) after several weld layers.

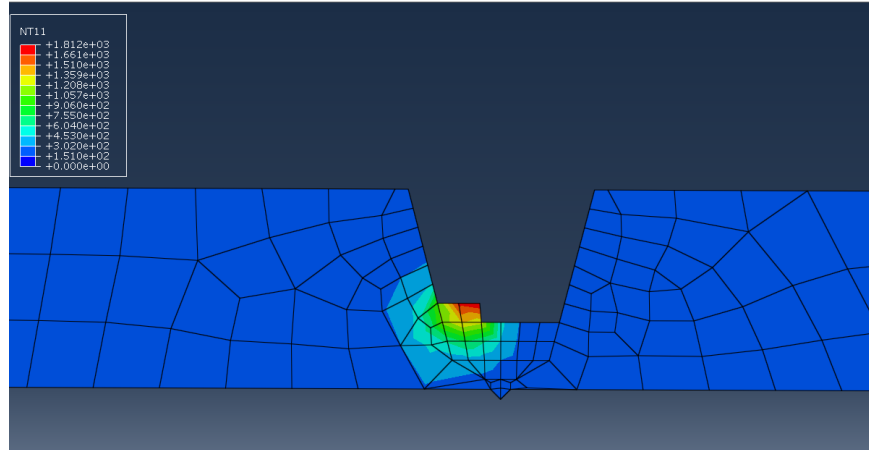


Figure 3. 3 Preliminary results showing the temperature distribution after few weld layers.

4 Publication Activities

Based on the previous LWRS work following on publications:

- a) Mohanty, S., Soppet, W. K., Majumdar, S. and Natesan, K. “Report on Assessment of Environmentally-Assisted Fatigue for LWR Extended Service Conditions”, March 2013, ANL/LWRS-13/1
- b) Mohanty, S., Majumdar, S., and Natesan, K., “Modeling Of Steam Generator Tube Rupture Using Extended Finite Element Method”, *Structural Mechanics in Reactor Technology (SMiRT)-22 conference*, San Francisco, California, USA - August 18-23, 2013 (The final paper accepted for publications in the SMiRT proceeding)

This page intentionally left blank



Nuclear Engineering Division

Argonne National Laboratory
9700 South Cass Avenue, Bldg. 208
Argonne, IL 60439

www.anl.gov



Argonne National Laboratory is a U.S. Department of Energy
laboratory managed by UChicago Argonne, LLC